Available online at www.sciencedirect.com
SCIENCE DIRECT®
International Journal of Heat and Mass Transfer 48 (2005) 227–234
International Journal of HEAT and MASS TRANSFER
www.elsevier.com/locate/ijhmt

Laser-induced micro-bubbles in cells

Dmitri Lapotko *, Ekaterina Lukianova

International Center, A.V. Luikov Heat and Mass Transfer Institute, 15, P. Brovka Street, Minsk 220072, Belarus

Available online 13 October 2004

Abstract

We report experimental study and detection of laser-induced micro-bubbles in individual live cells and in confined micro-volumes of solutions. Using pulsed laser radiation (532 nm, 10 ns) as the source of local heating we detected micro-bubbles in light-absorbing media that were caused at least by two mechanisms—heating of the media above (more than 300 °C) critical temperature (referred as 'hot' bubbles) and action of rarefaction pressure waves (referred as 'cold' bubbles) at much lower temperatures (30–150 °C). Bubble generation thresholds, probabilities of bubble forming and bubble lifetimes were experimentally studied with two photothermal (PT) methods—thermal lensing and PT-time-resolved imaging for human red blood cells, homogeneous solutions of haemoglobin, neutral red dye and for suspension of polystyrene nano-particles.
© 2004 Elsevier Ltd. All rights reserved.

Keywords: Bubble; Laser; Photothermal; Opto-acoustic; Cell; Damage; Spallation; Vaporization

1. Introduction

Biological damage during laser–tissue interaction at cell level is mainly associated with thermal phenomena. Among them the bubbles are considered as one of the most universal cause of cell damage [1–5]. Laser-induced bubbles are usually generated due overheating (hot bubbles) of local light-absorbing targets above critical temperatures (300 °C for water) [1,4–8]. Also the bubbles can be induced by rarefaction waves [9,10] that follow an absorption of short laser pulse [11–13] and such 'cold' bubbles may develop at temperatures much lower than those for vaporization. For example the bubbles in eye tissue were detected at 70–80 °C [10]. As for a cell level the conditions of generation of laser-induced bubbles still are rather unclear. Such situation is caused by technical problems related to quantitative measurement of thermal and acoustic phenomena in individual cells and in compatible micro-volumes. Experimental studies of hot and cold bubbles were done mainly for macro-samples that were not restricted by solid surfaces and that were much bigger in size. Cells have such specific features as very small heated volume (characteristic size of light-absorbing volumes may vary from 10 nm to 10 μm) and they are usually confined by solid walls of the sample chamber with non-absorbing fluid (this is typical when cells are studied with optical microscopes or flow cytometers). Also cells contain so many various inhomogeneities, which may stimulate bubble nucleation. The goal of our work was to investigate the conditions and potential mechanisms of generation of micro-bubbles inside individual cells and in confined micro-volumes of solutions under action of pulsed laser radiation and due to consequent non-stationary heat release in light-absorbing volume. Several samples

* Corresponding author. Tel.: +375 172 842 483; fax: +375 172 842 486.
E-mail address: ld@hmti.ac.by (D. Lapotko).

0017-9310/$ - see front matter © 2004 Elsevier Ltd. All rights reserved.
doi:10.1016/j.ijheatmasstransfer.2004.08.012

Nomenclature

C	the heat capacity	ΔT	the initial temperatures induced in a sample
N	number of irradiated objects (number of detected signals)	ΔT_v	difference between the vaporization temperature and the room temperature.
N_2	number of bubble-specific signals	α	the light absorption coefficient of media at the light wavelength
PR2	the probability of bubble occurrence	λ	the light wavelength
$R_{\min}$	minimal optically detectible radius	ε	the laser pulse fluence
R_p	radius of particle	$\varepsilon(0.5)$	bubble generation threshold
c_v	the heat capacity of water	ρ_p	the density of particle
c_p	the heat capacity of particle	ρ_v	the density of water
r_v	the heat of vaporization		

were studied: homogeneous media, nano-particles and individual RBC. Homogeneous media and particle suspension were used for modeling laser-induced thermal phenomena in cells, as the properties of model samples are known much better than those for the cells.

2. Methods and materials

2.1. Sample preparation and experimental model

Bubbles were generated by irradiation the sample (individual cell or some volume of homogeneous solution) with short focused single laser pulses with Gaussian intensity profile (532 nm, 10 ns duration at the level 0.5 of maximum, 7 μm diameter at the level 1/*e* of maximum). Such pulse parameters provided heat-confined condition when all absorbed energy is released within the absorbing volume before heat diffusion takes place. Photothermal microscope previously developed by us [14] was used for experiments. Four types of samples were studies.

(1) Individual red blood cells (RBC) were chosen as the cells with strong and spatially uniform light absorption by homogenous solution of hemoglobin at 532 nm. Cell diameter is 7 μm and thickness varies from 2 to 7 μm. Cells were obtained from fresh whole blood by its dilution with PBS by 450 times so that monolayer of individual cells was studied in sealed chambers (S–24737 by Molecular Probes Inc., Eugene, OR) between two parallel glasses—slide and cover glass on top (Fig. 1(a)). Slide was fixed at microscope stage so allowing positioning each cell into the center of laser beam. As the laser beam covers whole cell, after absorption of laser pulse the temperature in whole volume of the cell increases for the time comparable to laser pulse front (1–2 ns). After laser pulse termination the temperature of cell gradually decreases during 10–20 μs due to heat diffusion into surrounding solution.

(2) Solutions of the main RBC component—haemoglobin (Hb) was also prepared as homogeneous media from the same human RBC. Hb was separated from other proteins by gel filtration and ion exchange chromatography techniques [15]. The lyzate was introduced onto the chromatographic column with Sephadex G-100 (Pharmacia, Sweden). Hb-containing fractions were further purified on the chromatographic column with DEAE-cellulose (Sigma, USA) [16]. Purity of chromatographic fractions was verified with spectroscopic analysis. Selected fractions of Hb were combined and dialyzed against PBS overnight. Finally the solution of Hb was centrifuged for 15 min at 7000 g for separation of any aggregates and then were used in experiments.

Solution of Hb was studied as a sealed volume between two parallel glasses—slide and cover glass on top (Fig. 1(b)). Vertical gap between the two glasses was 6.8 μm by using polystyrene spherical particles (Spherotech Inc., Libertyville, IL) that were added into NR solution. Low concentration of these particles of specific size provided required gap (equal to particle diameter) between the glasses. Only particle-free areas of solution were irradiated by laser pulse. Preparation provided uniform absorption of laser pulse in the sample volume and excluded any potential local absorbers. In this case heated space was confined by laser beam diameter and vertical gap between the glasses.

(3) Homogeneous solutions with specified light absorption coefficient were prepared by diluting neutral red dye (NR) (Sigma-Aldrich Corp., St. Louis, MO) by distilled water. Light absorption coefficient for each NR concentration in the range 0.05–1 g/L was measured with spectrophotometer. The solution was studied as a sealed volume between two parallel glasses (Fig. 1(b))—slide and cover glass on top. Vertical gap between the two glasses varied as 0.6 μm and 6.8 μm by using polystyrene spherical particles (Spherotech Inc., Libertyville, IL) that were added into NR solution. Low concentration of these particles of specific size provided required gap (equal to particle diameter) between the glasses. Only particle-free areas of solution were irradiated by laser pulse. For a bigger gap between the glasses—120 μm—

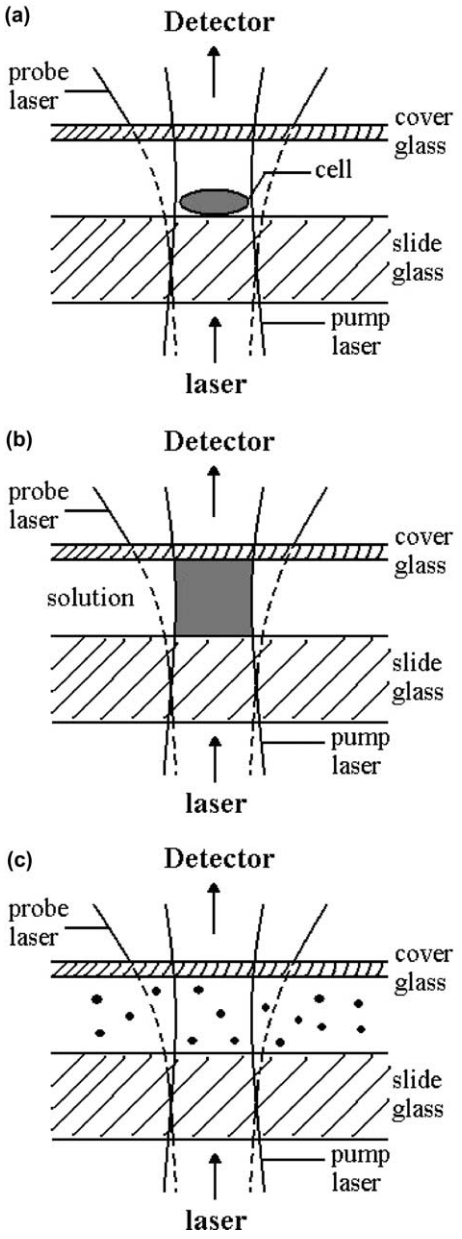

Fig. 1. Scheme of samples for study RBC (a), solution Hb (b) and suspension of nano-particles (c).

we have used gaskets between the glasses (S–24737 by Molecular Probes Inc., Eugene, OR). Additional filtering of NR solution provided sufficient homogeneity of this sample: first the solution was filtered through 0.22 μm micro-pore filters and then it was additionally centrifuged through 30 kDa filters. Such preparation provided uniform absorption of laser pulse in the sample volume and excluded any potential local absorbers. In this case heated space was confined by laser beam diameter and vertical gap between the glasses.

(4) This sample was principally different—we have prepared suspension of high-absorbing nano-particles in water to model local strong light absorption. Polystyrene blue particles of the diameter 180 nm, 390 nm, 500 nm (Spherotech Inc., Libertyville, IL) were prepared in the same geometry as for NR solutions (Fig. 1(c)). This type of sample was used as alternative to uniform light absorption because real cells may include local components with high absorption.

2.2. Detection of bubbles

Detection of laser-induced bubbles was performed using two photothermal methods—PT-response and PT-imaging with developed by us laser photothermal microscope [14]. Thermal lens method [17,18] provided registration of time-response (photothermal (PT)-response) of the whole irradiated volume with temporal resolution of 10 ns and thermal sensitivity 0.5 K. Heating–cooling process and the bubble produce different responses of specific shapes and in the case of bubble the duration of PT-response indicates bubble life-time and size [18]; PT-response was obtained by registering axial power of C.W. probe laser (633 nm, 0.1 mW, 15 μm diameter at sample plane) that was coaxially focused into the sample and after passing it was measured with aperture photodetector. Detector output signal $I(t)$ (Fig. 2) was registered and analysed for recognition the bubble and its lifetime. For time-resolved PT-imaging of laser-induced bubbles we have used coaxial probe laser pulse (640 nm, 8 ns, 15 μm diameter at sample plane) that was synchronized and delayed for 120 ns relatively to the pump pulse. So only the events that occurred 120 ns after pump pulse were illuminated and detected with CCD-camera with 8 ns integration time (Fig. 3).

In each sample 50–100 responses to laser pulse were obtained so each response represented one cell or one point of solution that was irradiated with only one pulse at specified energy (fluence). Then the probability of bubble occurrence was calculated as $PR2 = N_2/N$, where N—amount of irradiated objects, N_2—amount of bubble-specific responses [17,18]. The values of $PR2$ were obtained at several pulse fluencies so that the one corresponding to $PR2$ being 0.5 was defined as bubble generation threshold $\varepsilon(0.5)$ for a given sample.

2.3. Estimation of laser-induced temperatures

Initial temperatures that were induced in a sample after absorption of short laser pulse (all energy is released within absorbing volume) were calculated as

$$\Delta T(x,y) = \alpha(x,y,\lambda)\frac{\varepsilon(x,y)}{\rho C} \quad (1)$$

where α is the light absorption coefficient of media at the light wavelength λ (for RBC Hb concentration

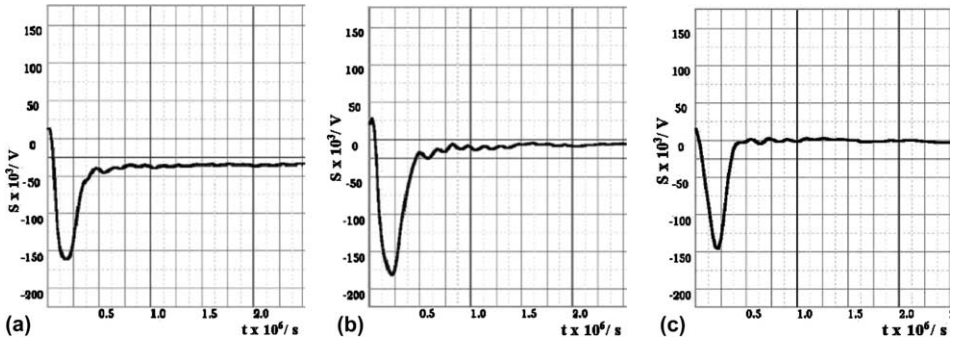

Fig. 2. PT-responses at 532 nm: (a) NR solution at concentration 0.9 g/L, 0.97 J/cm^2; (b) polystyrene particles (180 nm diameter), 2.7 J/cm^2 ; (c) RBC, 3.7 J/cm^2.

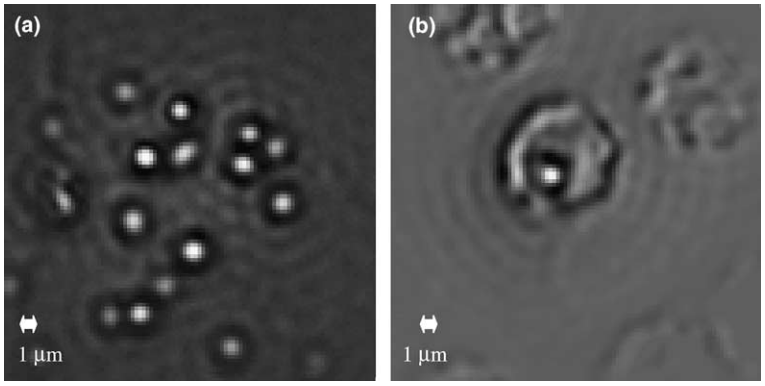

Fig. 3. PT-image of solution NR (0.83 J/cm^2, 532 nm, 0.1 g/L)—on the left and RBC (532 nm, 2 J/cm^2)—on the right.

339.9 ± 16.8 g/L [19], milimolar absorptivity of HbO_2 13,000 cm^{-1} M^{-1} [20], α (532 nm) = 135 cm^{-1}), ρ is the density (for RBC—1092 kg/m^3), ϵ is the laser pulse fluence, and C is the heat capacity (for blood its value is 3770 J/kg K). This expression was applied to homogeneous samples—RBC and NR solutions. For polystyrene particles an absorption coefficient was unknown (not provided by manufacturer and technically difficult to measure for individual particles). So minimal temperature of individual particle was derived from the balance of thermal energy that is required for vaporization of water volume with minimal optically detection radius (0.3 μm—this is a diffraction limit for light microscope with 20× micro-objective):

$$\Delta T = \left(\frac{R_{\min}}{R_p} - 1\right)^3 \cdot \left(\frac{\rho_v r_v + \Delta T_v c_v \rho_v}{c_p \rho_p}\right) \quad (2)$$

where $R_{\min}$ is the minimal optically detectible radius, R_p is the radius of particle, ρ_v is the density of water, r_v is the heat of vaporization, c_v is the heat capacity of water, c_p is the heat capacity of particle (1.76 kJ/kg K), ρ_p is the density of particle (1050 kg/m^3), ΔT_v is difference between the vaporization temperature and the room temperature.

3. Results

3.1. Thresholds for laser-induced bubbles

In all four studied samples the bubble-specific PT-responses (Fig. 2) and PT-images (Fig. 3) were detected when laser pulse fluence reached for the following thresholds ε(0.5): for RBC—2.81 J/cm^2, for Hb—19 J/cm^2 (at concentration 0.00015 M), for NR—0.97 J/cm^2 (at concentration 0.9 g/L), for the particles of the size 180 nm—2.7 J/cm^2 (at concentration 0.2%). These thresholds were measured as fluence values that correspond to 50% probability of bubble generation during laser-sample interaction. Shapes of PT-responses were rather similar for cells, solutions and particles (Fig. 2) reflecting the fact, that these responses are produced by the bubbles regardless the sample. Bubble-specific

PT-response has negative symmetrical profile which front describes bubble expansion and the tail describes bubble collapse. Length of bubble-related signal varied in the range from 0.2 μs (Fig. 2) to 7 μs (not shown). Visualization of the bubbles was accomplished with PT-imaging method by illuminating the sample with probe laser pulse of 10 ns length and delay of 120 ns. Diameter of the bubble for RBC and NR and Hb solutions at this stage (120 ns) may be estimated (see Fig. 3) as 1 μm. Value of delay (120 ns) seems to be shorter in comparison with the time when bubble radius reaches it's maximum (400–600 ns). Naturally at later times bubble diameter would increase so that the bubble may easily damage cell membrane. Unfortunately our experimental set up did not allow gradual variation of time-delay between probe and pump pulses. Images of the bubbles obtained for NR solution showed that several bubbles may develop simultaneously (Fig. 3(a)). In homogeneous media bubbles emerged in all area of the pump laser beam. The diameter of the bubbles is much smaller than that for heated volume (cell or laser beam). Number of the bubbles observed after single pump pulse varied from 1 to 4 with random location within the cell.

3.2. Bubble thresholds versus sample concentration

We have measured threshold fluence $\varepsilon(0.5)$ as function of mass concentration and of vertical thickness of the sample for Hb and NR solutions and for suspensions of particles (Fig. 4). Increase of mass concentration of absorbing molecules resulted in natural decrease of threshold fluence $\varepsilon(0.5)$ that reaches asymptotic saturation level when induced temperature is not enough for bubble generation, even if all laser energy is absorbed and converted into a heat. Threshold-concentration curves were quite similar for NR solution, Hb solution and for suspension of the particles. Also the particles yield another feature that was not found for molecular solutions—low concentration asymptotic behavior. This can be explained by discrete nature of the particles and finite volume of laser beam in sample chamber: with the decrease of particle concentration their amount within this volume may reach zero (no particles within the laser beam) so that no bubbles would emerge.

Table 1
Bubble probability PR2 as function of sample thickness

Vertical thickness $\times 10^6$/m	NR solution, $\varepsilon = 5.8$ J/cm^2	Particles (180 nm), $\varepsilon = 5.8$ J/cm^2
0.56	0.03	0
6.8	0.48	0.44
120	0.88	1

Increase of the thickness of absorbing volume (height of sample chamber) caused increase of bubble generation probability *PR2* both for solutions and suspension of particles (Table 1). This means that in both samples the mechanisms of bubble generation are volume-dependent. Also we found no change of bubble generation probability and thresholds for RBC in sample chambers of different height. This means that only height of absorbing volume influences those parameters of the bubbles but not the height of non-absorbing sample chamber.

3.3. Bubble lifetime versus laser fluence

The lifetime of laser-induced bubbles was measured for all samples as function of laser pulse fluence (Fig. 5 shows the results obtained for RBC). Increase of absorbed laser energy (and consequential increase of local temperature and pressure) caused an increase of bubble

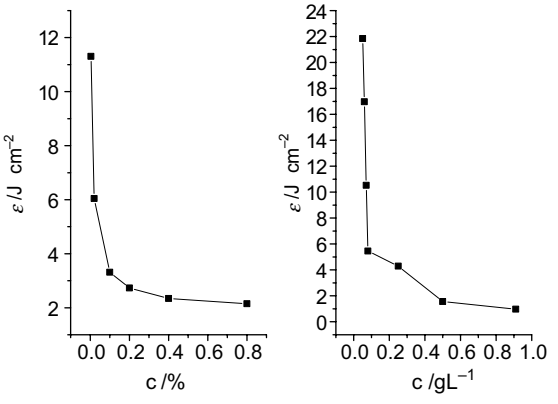

Fig. 4. Threshold fluence $\varepsilon(0.5)$ as function of mass concentration for NR solution (right) and for suspensions of particles of the size 180 nm (left).

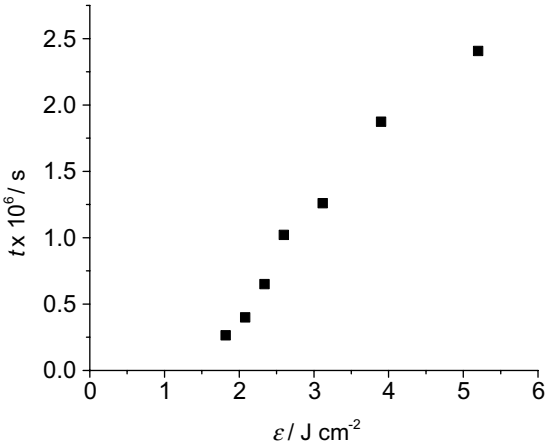

Fig. 5. The lifetime of laser-induced bubbles as function of laser pulse fluence for RBC.

lifetime for all studied samples. Minimal detected lifetime was about 100 ns and this is close to the detector temporal resolution (about 30 ns). Maximum lifetime was about 10 μs and this may be result of several oscillating bubbles. Therefore we may conclude about increase of maximal bubble radius with increase of laser fluence (increase of temperature). Also this function has threshold nature: at fluencies below critical value no bubbles were detected.

3.4. Reproducibility of the bubbles

We have studied reproducibility of the bubble generation when one cell or point of a solution is repeatedly irradiated with several laser pulses. The second laser pulse usually produced no bubbles in cells because they were destructed with the first pulse. Same result was obtained for low concentration of the particles when just several particles were present in irradiated volume. Apparently this is connected with thermal destruction of those particles by first pulse. In NR and Hb solutions and in suspensions of particles at higher concentration the bubbles were reproducible (according to PT-responses and PT-images) during at least 50 laser pulses with 1–3 s interval. This case is similar to low concentration of particles and to cells in terms of laser-induced temperatures: the damage of absorbing object will occur regardless concentration of absorber. But in case of NR and Hb solutions laser-induced heating may stimulate some convection that would pull new material into irradiated volume during the pause between two pulses (1–3 s). Same process would deliver new particles into the volume of laser-sample interaction when particle concentration is high enough.

3.5. Estimation of laser-induced temperatures

Using experimentally obtained threshold fluencies and the expressions (1) and (2) we have calculated initial laser-induced temperatures of studied samples (Table 2). The temperatures of the particles were above critical ones and are in line with current understanding of laser–tissue interaction as of selective local absorption and heating above critical temperatures. This is clear case for generation of thermal (hot) bubbles.

Table 2
Laser-induced maximal temperatures in studied samples at fluence corresponding to bubble thresholds

Sample	$\varepsilon(0.5)$/J cm^{-2}	ΔT/K
Solution NR 0.9 g/L[a]	0.97	31
Solution NR 0.05 g/L[a]	22	39
RBC[a]	3.7	91
Hb 0.00015 M[a]	19.1	184
P(180)[b]		18000
P(390)[b]		1750

[a] Here temperature was calculated with (1).
[b] Temperature was calculated with (2).

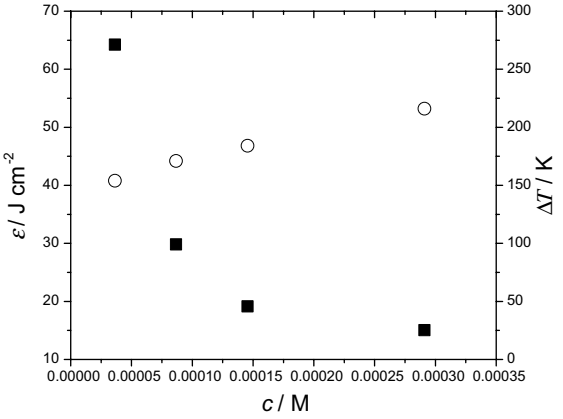

Fig. 6. Threshold fluence $\varepsilon(0.5)$ and laser-induced temperatures as function of concentration for Hb solution.

For RBC cells and especially for the solutions estimated initial temperatures were lower than critical value for water (above 300 °C) but the bubbles were detected at the temperatures being even 10 times lower than critical temperature. Furthermore the temperatures given in the Table 2 correspond to 0.5 probability of bubble generation. In same cells and solutions the bubbles were detected at even lower laser fluencies (temperatures) though at lower probabilities of their generation. Estimates for NR solutions were similar to each other in the whole range of concentrations (Fig. 4) and therefore they not depend upon it. Similar result was obtained for solution of Hb (Fig. 6). This means that in these solutions the bubbles are generated through some mechanism that works when some critical temperature is reached. Potential explanation can be connected with action of rarefaction waves—reaching for minimal negative pressure that is required for creating the cavity requires some minimal temperature.

4. Discussion

Analysis of numerous PT-images of cells and solutions showed that several bubbles may emerge simultaneously at different points. These points always were confined by the cell membrane or by pump beam diameter at sample plane in case of solution. The diameter of the bubbles at 120 ns delay was found to be much smaller than that of the cell (for RBC) or of the laser beam (for NR solution). Therefore the bubble nucleation occurs around heterogeneities that are much smaller than diameter of whole light-absorbing volume.

Closed glass chambers that are used for cell studies have several sound-reflecting solid walls. For that reason

acoustic signal that is induced by initial heating of absorbing volume and by the bubble will nave many echo components due to reflection from chamber walls. Also small size of absorbing volumes and also of sample chamber would result in very short (nano-second range) duration of acoustic bubble-related signals. Therefore acoustic detection of the bubbles that is usually applied in similar studies of macro-samples will require in our case very good temporal resolution (sub-nanosecond range) of acoustic detector and separation of the bubble-related signal from numerous echoes that may be mixed. For all of those reasons we assume that optical detection method that we applied is more reliable because it optical properties of the bubble and does not depend upon interference of acoustic waves in the sample chamber.

In our experiments the bubbles may be generated through three main mechanisms: overheating, spallation laser-induced heat release forms high pressure wave which crosses the cell and is followed by low pressure wave and optical breakdown. Optical breakdown requires reaching for laser intensity threshold of 10^{11} W/cm^2 (for the water). In our experiments maximal intensities were about 6.4×10^9 W/cm^2 that is below breakdown threshold. Also for this mechanism bubble generation threshold usually does not depend upon light absorption coefficient (concentration) of the sample though in our case such dependence was very strong. Therefore we may exclude optical breakdown as the mechanism for bubble generation.

Analysis of estimated temperatures shows that in he case of local strong light absorption the temperature exceeds critical value and therefore the bubbles would form due to overheating of the surrounding fluid. Our model with nano-particles is a good example when this mechanism provides bubble formation. But for the case of cells with uniform light absorption (RBC consist mainly of homogeneous Hb solution confined within cell membrane) and especially for solutions with low molecular weight (NR dye) laser-induced temperatures are not enough for burst vaporization. For this case we have estimated the levels of negative pressure in rarefaction wave that may occur after acoustic wave with positive pressure is induced by initial heating. For light-absorbing target with radius in the range 5–500 nm thermal relaxation times may vary from 1 to 1000 ns. Experimental data obtained with PT-imaging of cells and nano-particles a relaxation time of local sources of the PT-signal is about 100–1000 ns. The acoustic field relaxes within the cell during the time of about 1 ns, and laser pulse length is about 10 ns. These conditions are not good for effective pressure build up during action of laser pulse but such possibility still exists. We have applied spherical model suggested by Paltauf and Schmidth-Kloiber [21] for a pulse with a Gaussian temporal profile. Neglecting by heat conduction and viscosity we obtained for spherical object with size and absorption properties close to RBC in water the estimate of negative pressure about 20 bar. This is enough to create a cavity in water and thus to generate cavitation bubble. Currently we have not found among available sources the model of cavitations bubbles that can be applied to our samples (closed volume) and employ rarefaction wave. Development of such model is the subject of our ongoing studies. Nevertheless we may suggest that the two mechanisms of bubble generation may act simultaneously in such objects as cells and the role of each specific mechanism—overheating or spallation—depends upon degree of heterogeneity of cell structure in terms of light absorbance and in terms of thermal properties.

5. Conclusion

Generation of laser-induced bubbles in individual cells and in confined micro-volumes of solutions may be different from similar process in macro-samples and in samples with free surface. Two mechanisms are involved in bubble generation in confined micro-volumes and in individual cells—overheating and spallation. Laser-induced bubbles in absorbing samples may be much smaller in size (from nano-meters to micrometers) than the size of absorbing sample. Bubbles in cells may emerge at the temperatures below critical and therefore laser damage thresholds for specific tissue may be lower than that obtained under assumption of generation of the bubbles only through overheating mechanism. Detection of such bubbles can be done by optical means because acoustical signal from bubbles in cells can be difficult to detect due to influence of cell chamber with solid walls.

References

[1] S.L. Jacques, D.J. McAuliffe, The melanosome: threshold temperature for explosive vaporization and internal absorption coefficient during laser irradiation, Photochem. Photobiol. 53 (6) (1991) 769–775.

[2] J. Roegener, C.P. Lin, Photomechanical effects: experimental studies of pigment granule absorption, cavitation, and cell damage, in: G. Exarhos, A. Guenther, M. Kozlowski, K. Lewis, M. Soileau (Eds.) Laser-induced Damage in Optical Materials:1999, Proc. SPIE 3902 (2000) 35–40.

[3] R. Anderson, J. Parrish, Selective photothermollysisprecise microsurgery by selective absorption of pulsed radiation, Science 220 (4596) (1983) 524–527.

[4] B.S. Gerstman, C.R. Thompson, S.L. Jacques, M.E. Rogers, Laser induced bubble formation in the retina, Lasers Surgery Med. 18 (1) (1996) 10–21.

[5] C.P. Lin, M.W. Kelly, S.A.B. Sibayan, M.A. Latina, R.R. Anderson, Selective cell killing by microparticle absorption

of pulsed laser irradiation, IEEE J. Sel. Top. Quantum Electron. 5 (4) (1999) 963–968.

[6] J. Neumann, R. Brinkmann, Microbubble dynamics around laser heated microparticles, in: R. Steiner (Ed.), Therapeutic laser applications and laser–tissue interactions, Proc. SPIE. 5142 (2003) 82–87.

[7] V.K. Pustovalov, Thermal processes under the action of laser radiation pulse on absorbing granules inheterogeneous biotissues, Int. J. Heat Mass Transfer 36 (1993) 391–399.

[8] C.M. Pitsillides, E.K. Joe, X. Wei, R.R. Anderson, C.P. Lin, Selective cell targeting with light-absorbing microparticles and nanoparticles, Biophys. J. 84 (2003) 4023–4032.

[9] N.A. Inogamov, S.I. Anisimov, B. Retfeld, Rarefaction wave and gravitational equilibrium in a two-phase liquid–vapour medium, J. Exp. Theor. Phys. 88 (6) (1999) 1143–1150.

[10] G.I. Zheltov, A.S. Rubanov, Features of the destructive action on the eyes of near IR lasers, Report presented at Laser Bioeffects Meeting, Paris, France, (2002) 13–14.

[11] T. Juhasz, X.H. Hu, L. Turi, Z. Bor, Dynamics of shock waves and cavitation bubbles generated by picosecond laser pulses in corneal tissue and water, Lasers Surgery Med. 15 (1) (1994) 91–98.

[12] V. Venugopalan, A. Guerra III, K. Nahen, A. Vogel, Role of laserinduced plasma formation in pulsed cellular microsurgery and micromanipulation, Phys. Rev. Lett. 88 (7) (2002) 78–103.

[13] A. Vogel, S. Busch, K. Jungnickel, R. Birngruber, Mechanisms of intraocular photodisruption with picosecond and nanosecond laser pulses, Lasers Surgery Med. 15 (1) (1994) 32–43.

[14] D. Lapotko, G. Kuchinsky, Photothermal microscope, in: F. Scudiery, M. Bertolotti (Eds.), Photoacoustica and Photothermal Phenomena, AIP, Rome, 1998, pp. 184–186.

[15] E. Antononi, M. Brunoni, Hemoglobin and mioglobin and their reaction with ligands, North-Holland, Amsterdam, 1997.

[16] A. Kuki, S.G. Boxer, Chlorophyllide-substituted hemoglobin tetramers and hybrids: preparation, characterization, and energy transfer, Biochemistry 22 (12) (1983) 2923–2933.

[17] D. Lapotko, G. Kuchinsky, H. Antonishina, H. Scoromnik, Laser viability method for red blood cells state monitoring, in: H.-J. Foth, R. Marchesini, H. Podbielska, H. Schneckenburger, M. Robert-Nicoud (Eds.), Optical and Imaging Techniques for Biomonitorin, Proc. SPIE 2628 (1995) 340–345.

[18] D. Lapotko, K. Lukianova, A. Shnip, Photothermal detection of laser-induced damage in single intact cells, Lasers Surgery Med. 33 (5) (2003) 320–329.

[19] G. Aliberti, M. Proietta, I. Pulignano, C. Di Giovanni, L. Tritapepe, G. Vercillo, Respiratory changes in human red cells, Clin. Lab. Haematol. 23 (6) (2001) 361–363.

[20] E.J. van Kampen, W.G. Zijlstra, Spectrophotometry of hemoglobin and hemoglobin derivatives, Adv. Clinical Chem. 23 (1983) 199–257.

[21] G. Paltauf, H. Schmidth-Kloiber, Photoacoustic cavitation in spherical and cylindrical absorbers, Appl. Phys. A 68 (5) (1999) 525–531.